Applied Energy 107 (2013) 412–425

Contents lists available at SciVerse ScienceDirect

Applied Energy

journal homepage: www.elsevier.com/locate/apenergy

A hybrid tool to combine multi-objective optimization and multi-criterion decision making in designing standalone hybrid energy systems

A.T.D. Perera, R.A. Attalage *, K.K.C.K. Perera, V.P.C. Dassanayake

Department of Mechanical Engineering, University of Moratuwa, 10400 Katubedda, Sri Lanka

HIGHLIGHTS

- Mathematical modeling and simulation of a standalone hybrid energy system.
- Multi-objective optimization (MOO) considering techno-economical and environmental aspects.
- Using Fuzzy TOPSIS as a multi-criterion decision making (MCDM) technique.
- Proposing a decision making tool to combine MCDM, MOO and level diagrams.
- A case study using novel technique.

GRAPHICAL ABSTRACT

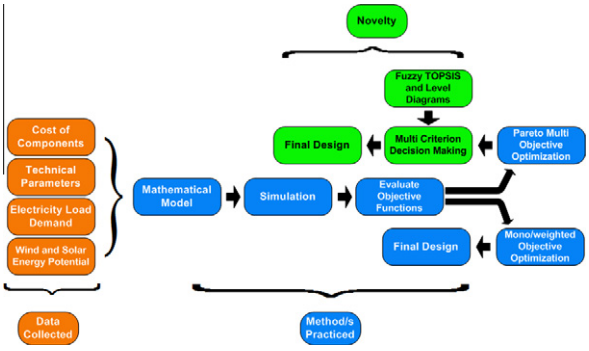

ARTICLE INFO

Article history:
Received 14 September 2012
Received in revised form 6 January 2013
Accepted 15 February 2013
Available online 20 March 2013

Keywords:
Hybrid energy systems
Standalone applications
Evolutionary multi-objective optimization
Multiple-criteria decision making
Fuzzy TOPSIS and level diagrams

ABSTRACT

Hybrid energy systems (HESs) are becoming popular for standalone applications due to global concern regarding green house gas (GHG) emissions and depletion of fossil fuel resources. Research in the optimal design of HESs is ongoing, with numerous optimization techniques giving special emphasis to Pareto optimization, incorporating conflicting objectives. The subsequent decision-making process including the non-dominant set of solutions has yet to be addressed.

This work focuses on combining multi-objective optimization with a multi-criterion decision making (MCDM) technique to support decision makers in the process of designing HESs. Four different objectives, i.e., levelized energy cost (LEC), unmet load fraction, wasted renewable energy (WRE) and fuel consumption are used to obtain the Pareto front. A decision support tool based on Fuzzy TOPSIS and level diagrams is proposed to analyze the Pareto front and support the subsequent decision-making activity. A case study is used to illustrate the applicability of the proposed method. The study shows that the novel method is useful when determining the relative weights of objectives, providing a detailed picture of the objective space to the designer when coming up with the optimum system. The technique proposed in this study can be further extended to analyze similar problems in energy system design where MCDM is necessary after multi-objective optimization.

1. Introduction

Ever increasing energy demands and the limitations of fossil fuel resources encourage energy system designers to come up with optimum designs. Various factors including vulnerability (safety and power security), environmental impact, sustainability issues and resource limitations must be considered when designing energy systems, requiring the simultaneous optimization of several factors [1]. As a result, the multi-objective optimization of energy systems has become a rich area of study [2]. Pareto multi-objective optimization has been used to optimize energy systems while

* Corresponding author. Tel.: +94 714964961; fax: +94 112650621.
E-mail address: dinu@mech.mrt.ac.lk (R.A. Attalage).

0306-2619/$ - see front matter © 2013 Elsevier Ltd. All rights reserved.
http://dx.doi.org/10.1016/j.apenergy.2013.02.049

Nomenclature

AA	area of SPV panel
A^-	Fuzzy Negative Ideal Solution
A^+	Fuzzy Positive Ideal Solution
AM	air mass
CRF	capital recovery factor
D^-	negative distance matrix
D^+	positive distance matrix
ELD	electricity load demand
f	rate of return on investment
FC(t)	fuel consumption hourly
FOM	fixed OM
FOM_{PV}	present value of FOM
G_β	hourly tilted solar irradiation
g	rate of local market annual inflation
HES	hybrid energy system
ICC_0	initial capital cost
ICG	internal combustion generator
J	benefit function
J'	cost function
LCC	life cycle cost
LEC	levelized energy cost
LPS	loss of power supply
MCDM	multi-criterion decision making
NPV	net present value
N_{SPV}	number of SPV panels
OM	operation and maintenance cost
$P_{Bat\text{-}Max}(t)$	maximum power of the battery bank
P_C	critical load
P_D	dispatch load
P_{min}	minimum ICG power
P_{ngen}	nominal power of ICG
P_r	rated power of wind turbine
$P_{SPV}(t)$	SPV power output
$P_w(t)$	wind power output
SOC	state of charge
SOC_{max}	maximum SOC
SOC_{min}	minimum state of charge
SPV	solar PV
TOPSIS	technique for order performance by similarity to ideal solution
V_{ci}	cut in wind speed
V_{co}	cutoff wind speed
VOM	variable OM
VOM_{PV}	present value of VOM
V_r	rated wind speed
w	weight matrix
WRE	waste of renewable energy
X	decision matrix
$\dot{x}$	normalize decision matrix
Y_w	weighted decision matrix
η_{Inv}	inverter efficiency
η_{pv}	SPV panels efficiency
θ_{cell}	cell temperature

considering aspects such as life cycle cost, energy/exergy efficiency and system reliability which helps to find a non-dominant set of solutions to be considered in the decision-making process [3,4]. However, a path that combines multi-objective optimization and decision-making is essential. Sayyaadi et al. [5] has discussed combining multi-objective optimization and decision-making using the Bellmane–Zadeh approach, considering life-cycle cost, pollutant emission and exergy efficiency as objective functions. However, with the increased number of objectives and ambiguous relative importance of those objectives, it is necessary to analyze the sensitivity of changing the weight of each objective [6]. This study focuses on combining multi-objective optimization and decision-making with a detailed analysis of the objective space for the design of a standalone hybrid energy system (HES).

HESs are becoming more popular worldwide every day for numerous applications, including rural power supply [7–9], telecommunications [10], desert agriculture [11], hotel industry [12,13] and desalination plant operation [14]. Compared to internal combustion generator (ICG) systems, HESs are eco-friendly and economical [15,16]. Nevertheless, designing an HES is a challenging endeavor, and a rigorous approach is required. Designing an HES consists primarily of two phases, i.e., selecting the optimum system configuration and determining the optimum system operating strategy [17]. Probabilistic, iterative and heuristic methods have been proposed to minimize the life cycle cost [18,19]. Recent reviews on the optimization of renewable energy systems show that heuristic methods are becoming more popular, especially for instances in which multi-criterion evaluation is required [2,4,20].

Several techno-economical factors must be considered in the HES design process. Therefore, multi-criterion evaluation becomes necessary, which can either be achieved through a weighted sum approach or Pareto optimization. Although it is easy to optimize a weighted objective function, it is difficult to understand the relative importance of each objective without knowing certain details of the objective space [6]. Therefore, it is essential to compute the non-dominant set of solutions through a Pareto multi-objective optimization, which portrays a more informative picture of the objective space. The multi-criterion decision making (MCDM) process can then be applied.

The concept of multi-objective optimization was first used by Dufo-López et al. [21] to optimize HESs considering the life cycle cost of the system and pollutant emissions as objective functions. Several works were published thereafter, studying different objectives of the design, including power supply reliability [22,23], pollutant emission [24] and utilization of renewable energy potential [18]. A recent study on the multi-objective optimization of HESs suggests the importance of identifying techno-economical parameters that match the local context and including them in the optimization process, where detailed analysis of alternative solutions is necessary [2]. This makes multi-objective optimization a tool that can be used to analyze the characteristics of HESs which was used by Bernal-Agustín et al. [25] to analyze the cost and life cycle emissions of solar PV–wind–ICG systems. Perera et al. [26] used multi-objective optimization techniques to analyze the impact of the ICG capacity in HESs, which discuss the role of dispatchable energy sources to minimize LEC while increasing power supply reliability. However, in regard to a particular application, it is necessary to go beyond the Pareto optimization and come up with a final system configuration. Therefore, it is necessary to combine multi-objective optimization and MCDM, and come up with a hybrid technique as highlighted by Bhattacharyya [27] that can be adapted to match with local context and application which is taken into consideration in this work.

Levelized energy cost (LEC), wasted renewable energy (WRE), fuel consumption and unmet load fraction are used as the evaluation parameters in this work, based on the recent research in HESs. A multi-objective optimization is performed to find the

non-dominant set of solutions using the above evaluation criteria. A detailed description of the mathematical model and the computational algorithm are given in Sections 2 and 3. The MCDM technique is described in Section 4 and the analysis of the results are presented in Section 5.

2. Mathematical modeling and simulation of the HES

Mathematical modeling of the HES combine a set of individual models in order to predict and analyze the overall performance of the HES [18,28]. A concise description about the mathematical model used for this study is presented in this section and a detailed version can be found in Ref. [26].

A standalone HES consisting of solar PV (SPV) panels, wind turbines, a battery bank and an ICG is modeled in this study in order to simulate and formulate objective functions (Fig. 1). When analyzing such a system, it is necessary to model energy flow, which can be used to derive objective functions such as power supply reliability, WRE and fuel consumption.

2.1. Modeling the SPV energy component

The hourly horizontal solar irradiation at Hambantota, (Fig. 2) where the HES is to be implemented, is modeled. The hourly tilted solar irradiation (G_β) values are calculated using Klutcher [29] and Climed-2 [30] models. Semi empirical formulae proposed by Durisch et al. [31] is used to calculate the efficiency of SPV panels (Eq. (1)).

$$\eta_{pv} = p\left[q\frac{G_\beta}{G_{\beta,o}} + \left(\frac{G_\beta}{G_{\beta,o}}\right)^m\right].\left[1 + r\frac{\theta_{\text{cell}}}{\theta_{\text{cell},o}} + s\frac{\text{AM}}{\text{AM}_o} + \left(\frac{\text{AM}}{\text{AM}_0}\right)^u\right] \quad (1)$$

where AM denotes the air mass and θ_{cell} is the cell temperature. The values of $G_{\beta 0}$, $\theta_{\text{cell},0}$ and AM_0 are taken as 1000 W m^{-2}, 25 °C and 1.5, respectively. Parameters p, q, r, s, m and u for different SPV technologies are taken from Ref. [32].

The hourly power output from the SPV panels ($P_{\text{SPV}}(t)$) is calculated using Eq. (2) taking panel area (A), efficiency of the inverter (η_{Inv}) and the number of SPV panels (N_{SPV}). N_{SPV} is optimized using the optimization algorithm.

$$P_{\text{SPV}}(t) = G_\beta \eta_{pv} A N_{\text{SPV}} \eta_{\text{Inv}} \quad (2)$$

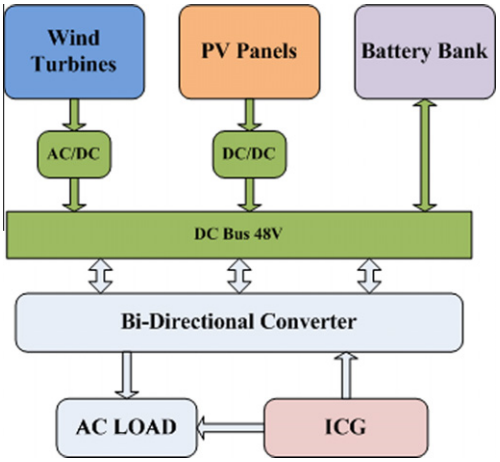

Fig. 1. HES configuration.

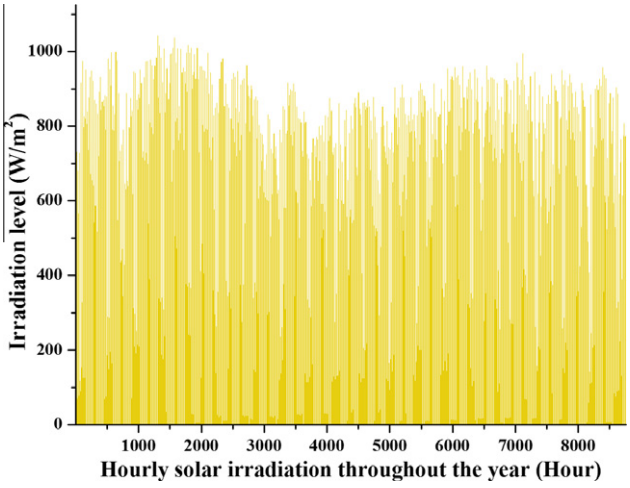

Fig. 2. Hourly variation of insolation at Hambantota.

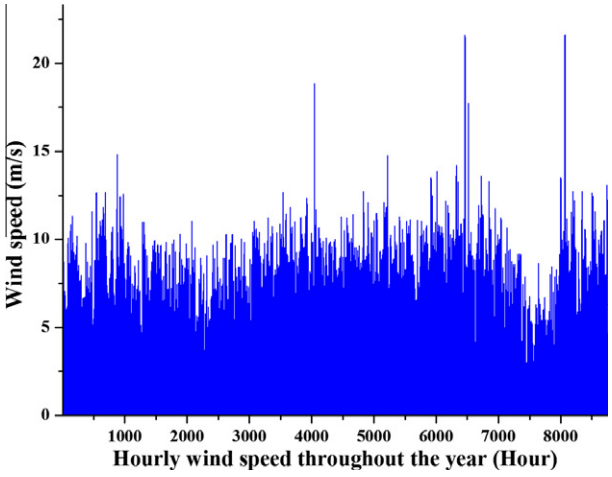

Fig. 3. Hourly variation of wind speed at Hambanthota.

2.2. Modeling wind energy component

Hourly wind speed (anemometer height of 10 m) throughout the year (Fig. 3) is measured at the same location. Based on that information, wind speed at the hub level (V) is calculated using the power law approximation to account for the atmospheric boundary layer. Wind speed at the hub level is used to calculate wind turbine power output, $\widetilde{P_w}(t)$ (kW/m^2) according to Eq. (3) [28,33].

$$\widetilde{P_w}(t) = \begin{cases} \widetilde{P_w}(t) = 0, & V < V_{\text{ci}} \\ \widetilde{P_w}(t) = aV^3 - bP_r, & V_{\text{ci}} < V < V_r \\ \widetilde{P_w}(t) = P_r, & V_r < V < V_{\text{co}} \\ \widetilde{P_w}(t) = 0, & V_{\text{co}} < V \end{cases} \quad (3)$$

where a and b are defined as: $a = \frac{P_r}{V_r^3 - V_{\text{ci}}^3}$, $b = \frac{V_{\text{ci}}^3}{V_r^3 - V_{\text{ci}}^3}$ and V_r, V_{ci}, V_{co} and P_r denote the rated wind speed, cut-in wind speed, cut-off wind speed and rated power of the wind turbine, respectively (Table 1).

Table 1
Specifications of the wind turbines.

V_{ci} (m/s)	V_r (m/s)	V_{co} (m/s)	P_r (kW)
3	12	20	Refer Table 3

Electric power from the wind turbines is calculated according to

$$P_W(t) = \widetilde{P_w}(t) A_W N_W \eta_{W-\text{inv}} \quad (4)$$

where A_W denotes the swept area of the wind turbine, N_W denotes the number of wind turbines that is optimized in the optimization algorithm and $\eta_{W\text{-inv}}$ denotes the inverter efficiency.

2.3. Modeling the battery bank and the ICG

The battery bank and the ICG work as dispatchable energy components, absorbing the fluctuations of the renewable energy potential. Therefore, the power requirement from the battery bank and the ICG depends on the dispatch strategy, as discussed in Section 2.4. Based on the power requirement, the load factor for the ICG is determined which is used to calculate the hourly fuel consumption (FC(t)), assuming that it varies linearly with the load factor [34,35], as shown in Fig. 4. The annual fuel consumption is calculated using

$$\text{FC} = \sum_{t=1}^{t=8760} \text{FC}(t) \quad (5)$$

In regard to the battery bank, the state of charge (SOC) model [36] is used to determine the charge level of the battery bank. The rain flow algorithm, based on Downing's algorithm [37], is used to estimate the lifetime of the battery bank. The inverter efficiencies are taken as 95%, assuming the variation of the load factor to be negligible [34].

2.4. Combined dispatch strategy

The combined dispatch strategy, which is a combination of the Battery-Charging strategy, the Frugal Discharge strategy, the SOC Set-point strategy, the Load Following strategy and the Peak Shaving strategy, is used in this model (Table 2) [35,38,39]. The operating state is mainly determined by the difference (PL(t)) between the electricity load demand (ELD) (Fig. 5) and the renewable energy produced (according to Table 2). The basic parameters of the dispatch strategy, such as the minimum state of charge (SOC_{min}), the minimum ICG power (P_{min}), the Critical load (P_C), the Dispatch load (P_D) and the SOC set point (SOC_{set}), were optimized.

The reliability of the power supply critically depends on the dispatch strategy. With respect to HES operation, the unmet load fraction has been used in several research studies to evaluate power supply reliability [22,23]. In this study, the unmet load fraction is used in the evaluation criteria of MCDM process and optimized in the optimization algorithm. Eq. (6) is used to calculate the loss of power supply (LPS).

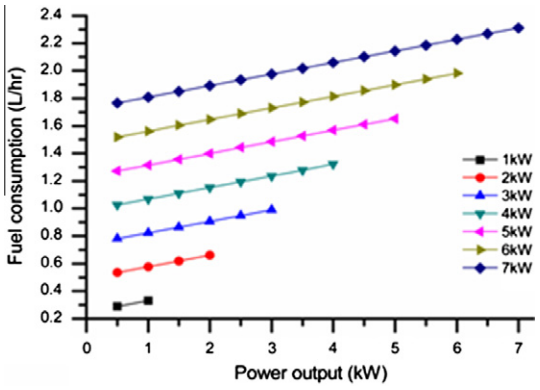

Fig. 4. Variation of fuel consumption with ICG load factor.

$$\text{LPS}(t) = \text{PL}(t) - P_{\text{ngen}} - P_{\text{Bat-Max}}(t) \quad (6)$$

where $\text{P}_{\text{Bat-Max}}(t)$ denotes the maximum power of the battery bank which depends on SOC(t). Finally, the unmet load fraction is computed using

$$\text{Unmet load fraction} = \sum_{t=1}^{t=8760} \text{LPS}(t) \Big/ \sum_{t=1}^{t=8760} \text{ELD}(t) \quad (7)$$

With the fluctuation of renewable energy potential, it is possible to generate energy that cannot be stored in the battery bank, resulting in poor energy efficiency. Therefore, it is essential to minimize WRE (Eq. (8)), which is also taken into consideration in the MCDM process and hence optimized in the optimization algorithm.

$$\text{WRE} = \sum_{t=1}^{t=8760} P_W(t) + P_{\text{SPV}}(t) - P_{\text{ELD}}(t) \forall t,\ s.t.\ P_W(t) + P_{\text{SPV}}(t) - P_{\text{ELD}}(t) \text{ and } \text{SOC}(t) = \text{SOC}_{\text{max}}(t) \quad (8)$$

2.5. Modeling of the cost elements

The life cycle cost (LCC) of the system consists of two components, i.e., the initial capital cost (ICC_0) and the operation and maintenance cost (O&M). The local market prices of system components used to come up with ICC_0 are tabulated in Table 3. The O&M cost comprises the fixed O&M (FOM) and variable O&M (VOM). The annual fuel consumption and maintenance costs of the ICG, wind turbines and SPV panels are considered FOM expenditures.

The present value of the entire FOM (FOM_{PV}) is computed using Eq. (9), where CRF denotes the capital recovery factor (Eq. (10)). In Eq. (10), p denotes the annual real interest rate and n denotes the lifetime of the project. The annual real interest rate, p, is calculated using Eq. (11), where f and g denote the rate of return on investment and annual inflation rate of local market, respectively (refer to Table 4).

$$\text{FOM}_{\text{PV}} = \text{FOM} \times \text{CRF} \quad (9)$$

$$\text{CRF} = (p(1-p^n))/(1-p) \quad (10)$$

$$p = (1+f)/(1+g) \quad (11)$$

The VOM includes the replacement cost of the battery bank, ICG and inverters. It is assumed that both the SPV and wind turbines have the same lifetime as that of the project. The net present value of the total VOM (VOM_{PV}) is calculated using

$$\text{VOM}_{\text{PV}} = \sum_{k=1}^{k=n} p^k \text{VOM}_k \quad (12)$$

The net present value (NPV) of the cash flow comprises ICC_0, FOM_{PV} and VOM_{PV} (Eq. (13a)), which is used to calculate the LEC according to Eq. (13b).

$$\text{NPV} = \text{FOM}_{\text{PV}} + \text{VOM}_{\text{PV}} + \text{ICC}_0 \quad (13a)$$

$$\text{LEC} = \text{LCC} \Big/ \sum_{k=1}^{k=n} \sum_{t=1}^{t=8760} \text{ELD}_{t,k} \quad (13b)$$

3. Multi-objective optimization algorithm

It is necessary to perform a Pareto multi-objective optimization to find the non-dominant set of solutions considering LEC, unmet load fraction, WRE and fuel consumption. Steady ε-state

Table 2
Concise description about dispatch strategy.

State	Range of PL(t)	Operation
State 1 Battery Charging	PL(t) < 0	Renewable energy is directed to supply the ELD and additional energy produced is used to charge the battery bank
State 2 Frugal Discharge	0 < PL(t) < P_D	ELD is higher than renewable energy production, Battery Bank is used to provide the additional energy required
State 3 SOC Set Point	P_D < PL(t) < P_C	ICG supply the additional energy requirement and is operated at its nominal power (P_{ngen}). Extra power produced is used to charge the battery bank until SOC Set Point is achieved
State 4 Load Following	P_C < PL(t) < P_{ngen}	ICG supply the additional power requirement following the load instead of charging the battery bank while operating at P_{ngen}
State 5 Peak Shaving	P_{ngen} < PL(t)	Both battery bank and ICG are used to supply the additional power requirement

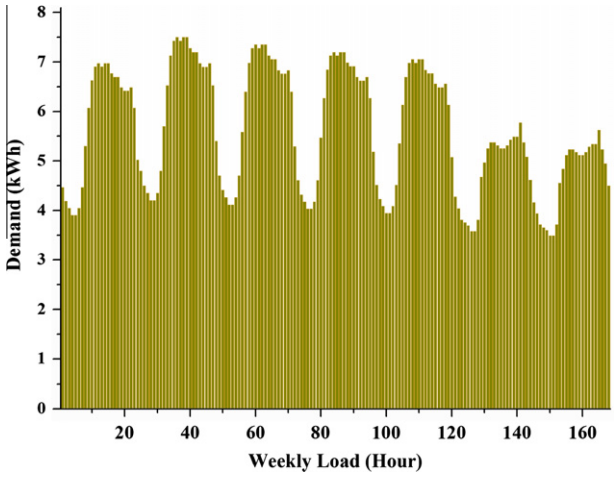

Fig. 5. Hourly variation of ELD based on summer – weekly load of IEEE reliability test system [60].

Table 3
Market prices of system components.

Component	Description	Cost (US $)
Wind turbine (20 year life time)	3 kW (P_r)	16,000
	5 kW (P_r)	20,000
Solar panels (20 year life time)	Mono-Crystalline (1.22 m^2)	1113
	Poly-Crystalline (0.79 m^2)	1128
	Amorphous(1.28 m^2)	1404
ICG	0.5 kV A–7.5 kV A (single phase) (20,000 working hours)	335.5–4195
	Hourly O&M	0.16
Cost of fuel	(Diesel 1 L)	0.8
Battery	12 V, 250 Ahs	580
Inverter	Single phase 10 kW (4 years lifetime)	1300

Table 4
Parameter values of the cost model.

Parameter	Percentage (%)
Rate of return on investment (f)	8
Annual fuel inflation rate	6
Local market annual inflation rate (g)	2

evolutionary algorithm [40] based on the ε-dominance method [41] is used as the optimization algorithm. The simulated binary crossover operator and the polynomial mutation operator are used as the crossover and mutation operators [42]. The constraint of 20% unmet load fraction is set to make the analysis trouble-free (refer Table 5). Constraint tournament technique is incorporated into the optimization algorithm [43] in order to support constraint multi-objective optimization.

3.1. Decision space variables

Parameters related to both the system configuration and operation strategy are incorporated into the decision space. A vector that includes the number and type of wind turbines, the number and type of solar panels, the number of batteries in the battery bank and the ICG capacity is used to insert variables into the optimization algorithm (Table 5). Variables related to the operational strategy, such as P_C, P_D, SOC_{Set}, minimum depth of discharge (SOC_{min}) and minimum generator power (P_{min}), are selected as shown in Table 5.

3.2. Optimization algorithm

The initial population is randomly generated in the optimization algorithm and the objective function values are subsequently evaluated. The non-dominant set of solutions is identified, and an initial archive is formed based on the objective function values. Members are selected randomly from the archive and population, and reproduction of the population and archive is performed through mutation and crossover operations. Subsequently, values of the objective function are evaluated, and the population and archive are updated. This routine is followed until the termination from the main loop, which take place when the desired generations of the algorithm has been reached (Fig. 6). Parameters such as crossover and mutation rates are taken according to Table 6.

4. Multi-criterion decision making technique

Decision-making plays an important role when designing energy systems that combine technical, financial, social and environmental aspects. In most cases, alternative sets of solutions can be obtained immediately, and the MCDM technique can be applied directly. However, in regard to HES design, a lengthy procedure is necessary to arrive at the alternative set of solutions, including modeling, simulation and multi-objective optimization (Fig. 7). The objective functions need to be modeled and simulated on an hourly basis to compute the objective function values. Further, multi-objective optimization must be performed in order to find the non-dominant set of solutions. Finally, MCDM technique can be applied to find the final system design.

With respect to energy system design, many MCDM techniques have been used, including the weighted sum method, the analytical hierarchical process (AHP) and the Fuzzy-TOPSIS (technique for order performance by similarity to ideal solution) [44,45]. Compared to other techniques, Fuzzy TOPSIS is capable of handling the ambiguity associated with the relative importance of objective functions (objective space) through the help of fuzzy set theory in

Table 5
Decision space variables, objective functions and constraint.

Decision space variables				Objective functions	Constraint
Variable	Minimum	Maximum	Interval		
SPV Type	0	3	1	LEC unmet fraction fuel consumption WRE	Unmet fraction <20%
SPV Panels	0	220	1		
Wind turbine type (3 kW, 5 kW)	0	2	1		
Wind turbines	0	20	1		
No of batteries	0	100	4		
ICG Capacity	0	7.5	0.5		
SOC_{min}	30%	50%	Continuous		
P_{min}	30%	50%	Continuous		
SOC_{set_value}	70%	100%	Continuous		
P_D	P_{min}	P_{ngen}	Continuous		
P_C	P_D	P_{ngen}	Continuous		

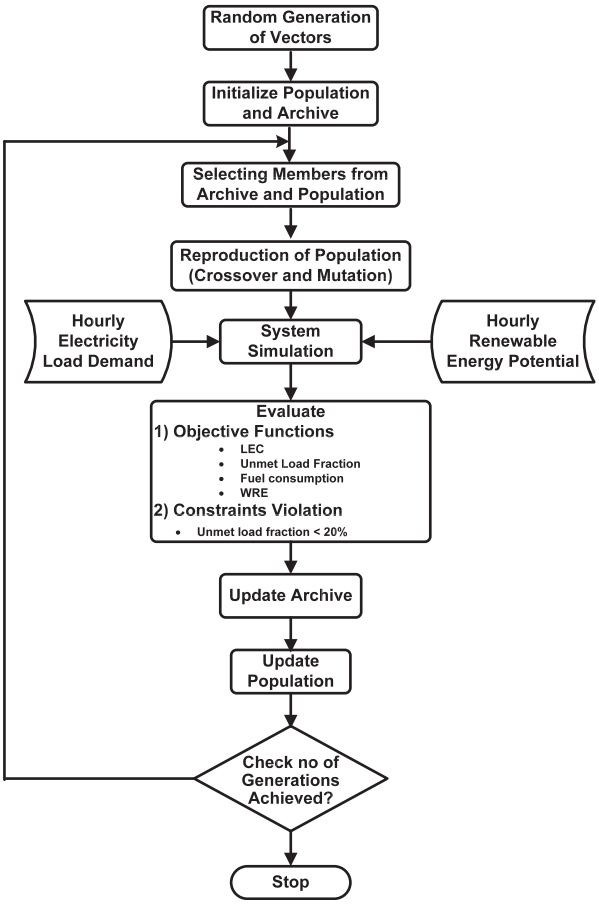

Fig. 6. Optimization algorithm.

the decision-making process [46]. Therefore, it is used in wider spectrum of applications including supply chain management and logistics [47,48], manufacturing systems design [49], business and marketing management [50] and energy system design [51,52]. A detailed description about various applications of Fuzzy TOPSIS can be found in recent review of Behzadian et al. [53] on applications of Fuzzy TOPSIS.

4.1. Fuzzy TOPSIS

The Fuzzy TOPSIS method follows several steps in the decision-making process, described in this section.

Table 6
Parameter values of the evolutionary algorithm.

Crossover rate	Mutation rate	η_c	η_m	ε	Generations
0.90	0.1	1	100	0.002	200,000

Step 1: Constructing the decision matrix

General problems related with MCDM involve m alternatives evaluated with respect to n criteria, which can be concisely expressed through a (mxn) matrix, known as a decision matrix, according to

$$X = \begin{pmatrix} x_{11} & x_{12} & \cdots & x_{1n} \\ x_{21} & x_{22} & \cdots & x_{2n} \\ \cdots & \cdots & \cdots & \cdots \\ x_{m1} & x_{m2} & \cdots & x_{mn} \end{pmatrix} \begin{matrix} \rightarrow \text{Criteria} \\ \downarrow \text{Alternatives} \end{matrix} \quad (14)$$

In the decision matrix, x_{ij} represents the significance of the ith alternative solution with respect to the jth criterion. Objective functions, i.e., LEC, unmet load fraction, fuel consumption and WRE, are the basis of the evaluation (described in Step: 3).

Step 2: Normalization of the decision matrix

The decision matrix is normalized to eliminate anomalies. In this problem, all four objectives are to be minimized. Therefore, a simple linear transformation, shown in Eq. (15), is used to derive the normalized decision matrix, $\dot{x}$.

$$\dot{x}_{ij} = \frac{x_{i,j} - x_{\min,j}}{x_{\max,j} - x_{\min,j}} \quad (15)$$

where $x_{\min,j}$ and $x_{\max,j}$ denote the minimum and maximum values, respectively, that can be obtained for the alternatives (Table 7) with respect to the jth criterion.

Step 3: Constructing the fuzzy decision matrix

Alternatives are rated based on the normalized objective function values using triangular fuzzy numbers to construct the fuzzy decision matrix. Weights are subsequently assigned to construct the fuzzy decision matrix, as shown in Table 8. The specialty of this work is that the rating is based on the normalized objective function value instead of by the decision makers.

Step 4: Constructing the weighting matrix

The weighting matrix is used to estimate the relative importance of each objective according to

$$W = (w_1 w_2 \ldots w_n)_{1\times n} \quad (16)$$

Step 5: Constructing the weighted decision matrix

The weighted decision matrix (mxn), Y_w, is computed using the weighting matrix according to

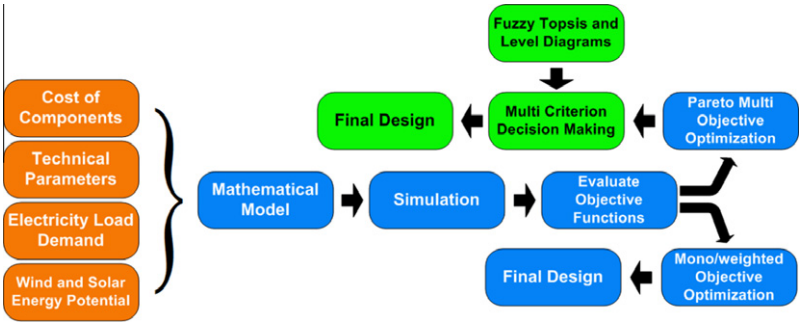

Fig. 7. Complete design process from modeling to MCDM.

$$Y_w = \begin{pmatrix} \breve{v}_{11} & \breve{v}_{12} & \cdots & \breve{v}_{1n} \\ \breve{v}_{21} & \breve{v}_{22} & \cdots & \breve{v}_{2n} \\ \cdots & \cdots & \cdots & \cdots \\ \breve{v}_{m1} & \breve{v}_{m2} & \cdots & \breve{v}_{mn} \end{pmatrix} \tag{17}$$

where $\breve{v}_{ij} = w_i \times \dot{x}_{ij}$

Step 6: Determining the Fuzzy Positive Ideal Solution (A^+) and the Fuzzy Negative Ideal Solution (A^-)

Eqs. (18) and (19) are used to determine A^+ and A^-.

$$A^+ = \begin{cases} \max_i & \breve{v}_{ij} | \forall j \in J \\ \min_i & \breve{v}_{ij} | \forall j \in J' \end{cases} \tag{18}$$

$$A^- = \begin{cases} \min_i & \breve{v}_{ij} | \forall j \in J \\ \max_i & \breve{v}_{ij} | \forall j \in J' \end{cases} \tag{19}$$

where J and J' represent benefit and cost functions, respectively. In this problem, all objective functions are to be minimized and can be treated as cost functions

Step 7: Deriving the distance matrix

The positive distance matrix, D^+ $(1 \times n)$, and the negative distance matrix, D^- $(1 \times n)$, are calculated using the Euclidian distance between A^+ and A^-, the elements of the weighted decision matrix and Eqs. (20) and (21).

$$D_i^+ = \left\{ \sum_{k=1}^{n} (A_k^+ - V_{ki})^2 \right\}^{0.5} \tag{20}$$

$$D_i^- = \left\{ \sum_{k=1}^{n} (A_k^- - V_{ki})^2 \right\}^{0.5} \tag{21}$$

Step 8: Deriving the coefficient of closeness

Relative closeness to the ideal solution is calculated using the coefficient of closeness (CC), which is used to rank the alternatives. CC $(1 \times m)$ is calculated by using

$$CC_i = \frac{D_i^-}{D_i^- + D_i^+} \tag{22}$$

4.2. Level diagrams

Level diagrams [54] can be used to support decision makers when estimating the weight matrix. A level diagram is based on the classification of the Pareto front approximation according to the proximity to the ideal point. Level diagrams have been used for number of applications including system redundancy allocation [55], design of nuclear systems [56], PI [57] and PID [58] controllers, data clustering [59], etc.

However, for this problem, the level diagrams need to be combined with Fuzzy-TOPSIS. Therefore, CC was used instead of the 1-norm or infinite norm.

5. Results and discussion

It is a challenging process to find the optimum system that meets all the design requirements. LEC, power supply reliability, WRE and fuel consumption are used as the evaluation criteria, covering techno-economical and environment factors related to the design. Selecting the correct weight matrix for the set of objectives is the most difficult consideration for the designer.

5.1. Sensitivity of the weight matrix

To analyze the impact of the weight matrix on the final design, three cases with different weight matrices are compared, as shown in Table 9. Level diagrams and best alternatives (groupings of six) for each weight matrix are compared to support the analysis.

Table 7
Minimum and maximum objective function values used to normalize.

	$x_{\min,j}$	$x_{\max,j}$
LEC	0.3166	1.0391
Unmet fraction (%)	0	19.86
Fuel (L/yr)	0	6583.14
WRE (MW h/yr)	0.056	48.24

Table 8
Linguistic rating and weights assigned.

Normalized objective function value	Linguistic rating	Triangular fuzzy number for rating	Triangular fuzzy number for importance weight
(0,0,0.3)	Poor	(0,0,3)	(0,0,0.3)
(0.3,0.5,0.7)	Average	(3,5,7)	(0.3,0.5,0.7)
(0.5,0.7,1.0)	Good	(5,7,10)	(0.5,0.7,1.0)
(0.7,10,10)	Very Good	(7,10,10)	(0.7,10,10)

Table 9
Weight matrix for three cases.

Rank	LEC	Unmet fraction	Fuel consumption	WRE
Case 1	0.5	0.3	0.1	0.1
Case 2	0.5	0.3	0.12	0.08
Case 3	0.8	0.05	0.1	0.05

The top six alternatives for Case 1 are tabulated in Table 10. When comparing these solutions, slight changes can be observed in the objective functions. More importantly, the first and the fifth are the alternatives that have the minimum LEC among the six. These two show the impact of other factors, such as unmet load fraction, WRE and fuel consumption, when arriving at the final design. When analyzing the decision space variables of the alternatives, the first and third alternatives are having similar system configurations. With respect to decision space variables, all of the systems are having a 5 kV A capacity ICG. However, the variation of the SPV capacity is significant compared.

To evaluate the sensitivity of the weight matrix further, two different weight matrices were taken, where Case 2 is marginally different from Case 1. When comparing Case 2 (Table 11) with Case 1, it is observed that even a slight change in the weight matrix can influence the final solution. For example, the weight of the LEC is constant when moving from Case 1 to Case 2. However, changes of the weights related to WRE and fuel consumption result in a noticeable increase in LEC in the final solution. Even though the weight of the unmet load fraction is kept constant, the unmet load fraction of the final solution decreases from 0.063% to 0.057%. In regard to the HES design, a small change in the number of SPV panels and battery banks is observed. Therefore, it is clear that the sensitivity of the weight matrix is notable for both objective functions and the final system design.

With respect to Case 2 (Table 12), a significant change is introduced to the weight matrix in Case 3, and resultant changes can be observed in both objective function values and the system configuration. LEC decreases by a considerable amount while increasing the unmet load fraction. In both Case 1 and Case 2, the unmet load fraction is less than 0.07%, and in Case 3, the best alternative has an unmet load fraction of 7.07%, an order of magnitude increase. Moreover, both Case 1 and Case 2 have 5 kV A ICGs, which is reduced to 1.5 kV A in Case 3. Further, a significant drop in SPV capacity is observed. These results, illustrates the impact of the weight matrix on the final system configuration and the importance of matching it with the requirements of the application.

5.2. Level diagrams used to support decision making

Sensitivity of the weight matrix is significant in determining the final system configuration. Therefore, it is further analyzed using level diagrams. Level diagrams of Case 1 and Case 3 provide a general idea about the impact of the weight matrix on the final design (Fig. 8). In the level diagram of the unmet load fraction for Case 1, the global maximum (CC) is reached when the normalized unmet load fraction is 0.003, and there is a local maximum in the range of 0.2–0.3. These results indicate that a reduction in the weight of the unmet load fraction could have a significant impact on power supply reliability. When moving from Case 1 to Case 3, the weight of the unmet fraction is reduced, and subsequently, the global maximum and local maximum in the unmet load fraction has interchanged as expected (refer to Fig. 8). The level diagram of the LEC exhibits a gradual gradient. Therefore, the

Table 10
Top six alternatives for the weight matrix of Case 1.

Rank	D_i^-	D_i^+	CC_i	LEC ($)	Unmet fraction (%)	Fuel (L/yr)	WRE (MW h/yr)	SPV[a] panels	Wind[b] turbines	ICG capacity (kV A)	Battery banks
1	9.44	0.72	0.9291	0.4707	0.0626	2289	9.96	47	5	5	26
2	9.42	0.72	0.9290	0.4985	0.0411	2117	6.84	65	4	5	27
3	9.41	0.72	0.9289	0.4983	0.0566	1997	11.42	55	5	5	28
4	9.41	0.73	0.9280	0.4743	0.0487	2183	14.82	38	6	5	27
5	9.43	0.74	0.9272	0.4571	0.0704	2327	14.47	35	6	5	23
6	9.39	0.75	0.9260	0.5176	0.0442	2007	6.96	67	4	5	33

[a] SPV panels with Amorphous type.
[b] Wind turbine with 5 kW capacity.

Table 11
Top six alternatives for the weight matrix of Case 2.

Rank	D_i^-	D_i^+	CC_i	LEC ($)	Unmet fraction (%)	Fuel (L/yr)	WRE (MW h/yr)	SPV[a] panels	Wind[b] turbines	ICG capacity (kV A)	Battery banks
1	9.40	0.72	0.9289	0.4983	0.0566	1997	11.42	55	5	5	28
2	9.42	0.74	0.9272	0.4707	0.0626	2289	9.96	47	5	5	26
3	9.41	0.74	0.9271	0.4743	0.0487	2183	14.82	38	6	5	27
4	9.41	0.74	0.9271	0.4985	0.0411	2117	6.84	65	4	5	27
5	9.42	0.75	0.9263	0.4571	0.0704	2327	14.47	35	6	5	23
6	9.37	0.76	0.9250	0.5157	0.0313	1795	12.56	61	5	5	28

[a] SPV panels with Amorphous type.
[b] Wind turbine with 5 kW capacity.

Table 12
Top six alternatives for the weight matrix of Case 3.

Rank	D_i^-	D_i^+	CC_i	LEC ($)	Unmet fraction (%)	Fuel (L/yr)	WRE (MW h/yr)	SPV[a] panels	Wind turbines[b]	ICG capacity (kV A)	Battery banks
1	9.3	0.76	0.9245	0.439	7.07	2105.17	15.2	25	6	1.5	19
2	9.26	0.76	0.9242	0.458	5.98	2134.33	12.42	43	5	1.5	16
3	9.31	0.77	0.9236	0.4352	7.39	2202.24	10.95	35	5	1.5	16
4	9.3	0.77	0.9235	0.4383	7.35	2134.32	14.79	23	6	1.5	21
5	9.25	0.78	0.9222	0.4579	5.74	2015.03	17.04	34	6	1.5	16
6	9.25	0.78	0.9222	0.4579	6.4	2172.44	11.44	39	5	1.5	21

[a] SPV panels with Amorphous type.
[b] Wind turbine with 5 kW capacity.

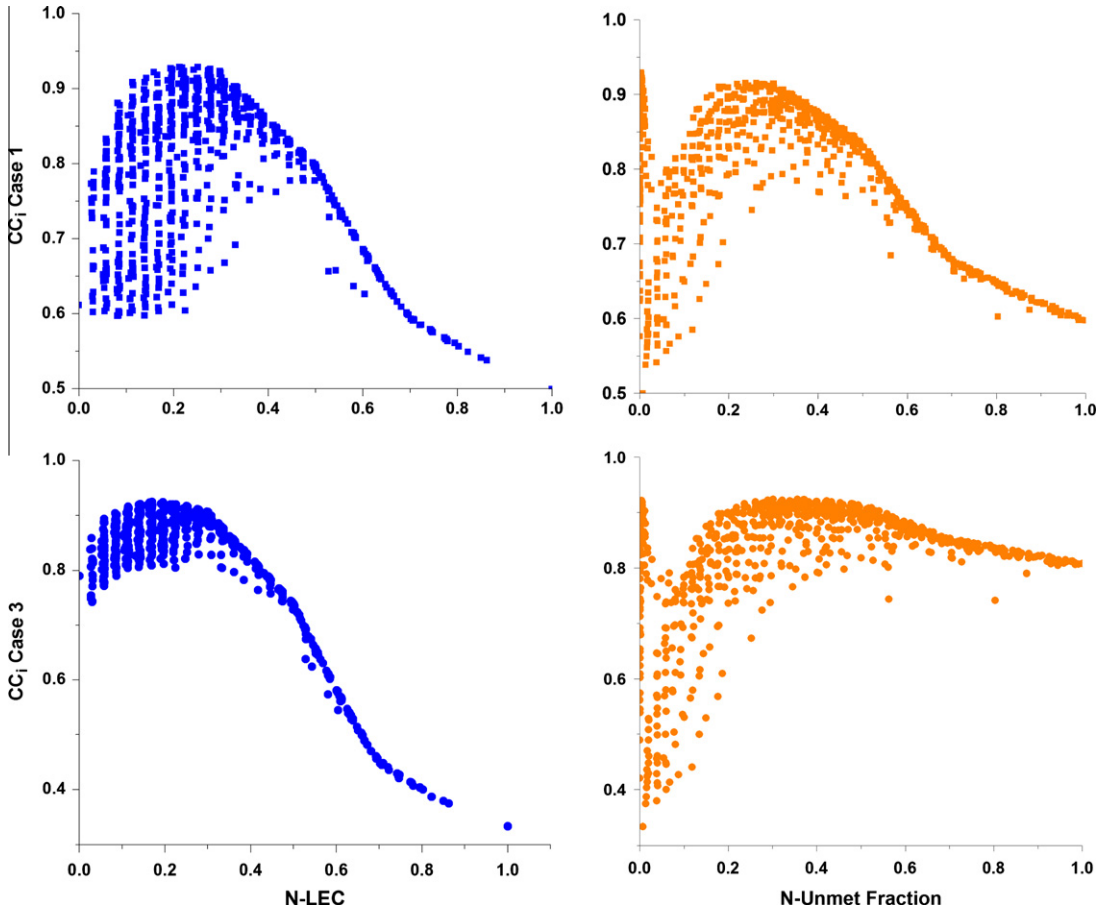

Fig. 8. Comparison of level diagrams for Case 1–Case 3.

impact of the weight matrix on the LEC is trivial compared to that on the unmet load fraction. For example, when moving from Case 1 to Case 3, N-LEC has reduced from 0.213 to 0.169, which is trivial compared to the same value for the unmet load fraction. These results show that level diagrams provide a good overall picture about the variation of CC with the normalized objective functions and support the development of the weight matrix.

Nevertheless, there are certain limitations, even with level diagrams. Even though level diagrams provide a general idea of the impact of the weight matrix, 1-D level diagrams cannot be used to fine-tune the weight matrix. For example, when moving from Case 1 to Case 2, it is difficult to find a notable change in the level diagrams (Fig. 9). In such instances it is essential to move towards 2-D level diagrams which is discussed in detail in next section.

5.3. Decision-making process

According to the novel method proposed in this study, multi-objective optimization of the HES is the initial step of the design process. After deriving the non-dominant set of alternative solutions, multi-criterion decision making becomes the second stage, which comprises several steps (Fig. 10). At the beginning, decision makers must deduce the upper boundaries of the objective space while considering special design requirements. The initial weighting matrix can be taken subsequently. An iterative process is introduced in this study to fine-tune the weight matrix which is discussed in detailed through a case study.

With respect to ranking alternatives, it is essential to identify the upper limits related to objective functions, including design requirements (Fig. 10). Contour plots of the Pareto front are generated to find the upper bounds of the objective functions (Figs. 11 and 12) as the initial stage. In this design, higher power supply reliability is expected while minimizing LEC, which is taken as a special design requirement. Finally, upper bounds were finalized according to Table 13, which may vary with the application.

Initial weight matrix is taken according to Table 14 (Case 4) after going through the contour plots. Subsequently, the CC of the alternatives is calculated. Then, level diagrams of the alternatives are plotted (Fig. 13), and the best six alternatives are tabulated (Table 15) using the MCDM process outlined in Fig. 10. The next step is the analysis of the Pareto front. When analyzing the level diagram of the unmet load fraction and fuel consumption, local maxima can be observed (Fig. 13). These local maxima indicate that significant reductions in unmet load fraction and fuel consumption can be achieved by adjusting the weight matrix (Section 5.2).

Therefore the weight matrix is changed according to Case 5 (Table 15) in order to increase the power supply reliability. As the weight related to power supply reliability increases, a significant increase in power supply is observed (Fig. 13). The best six alternatives for Case 5 are shown in Table 16. When analyzing the best six alternatives, it is clear that all of them are within the bounds set initially.

However, further changes can be made to optimize the design, which cannot be analyzed through 1-D level diagrams. Therefore, contour plots are constructed to consider two objectives at a time, along with CC (2D level curve). Since the LEC and the unmet load fraction are higher priority factors, a contour plot of LEC, unmet load fraction and CC is examined first. Maxima can be observed in the contour plot in the areas of A and B in Fig. 14. When analyzing the best set of alternatives in Table 16, it is clear that the global

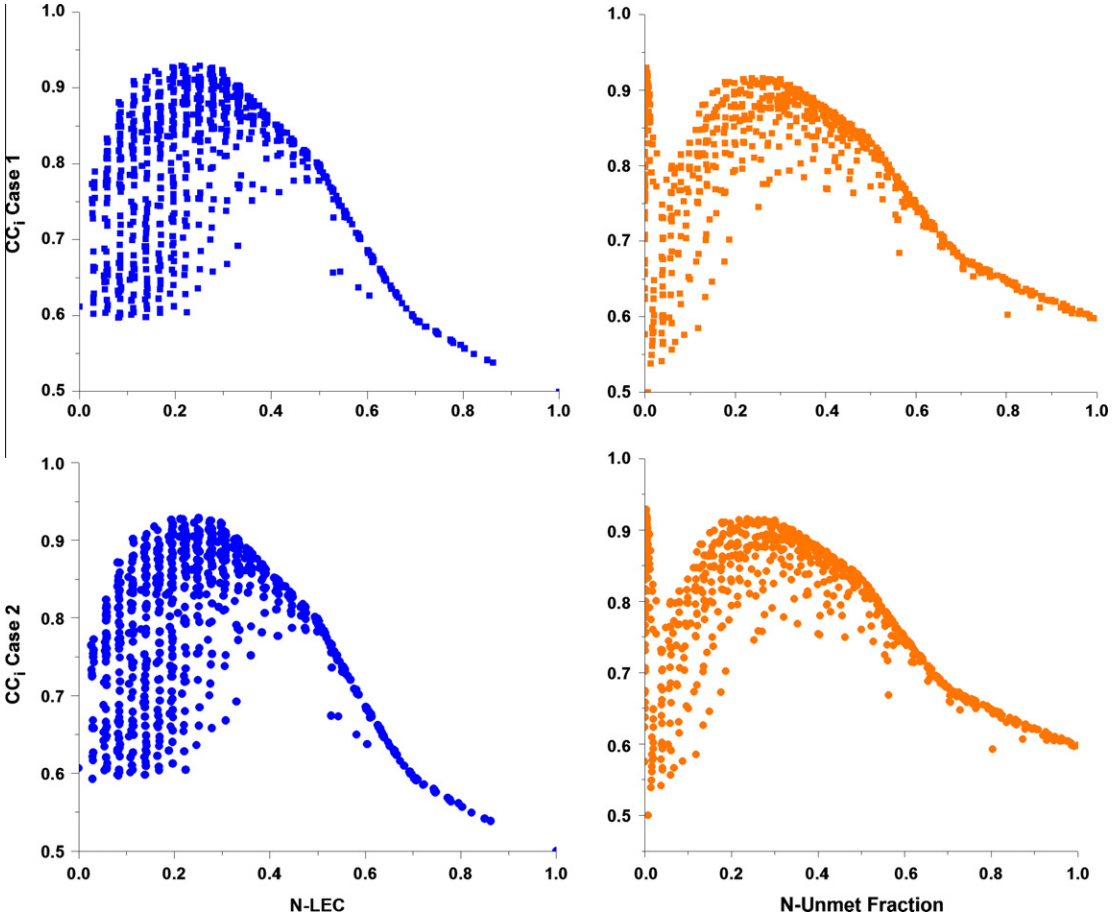

Fig. 9. Comparison of level diagrams for Case 1 and Case 2.

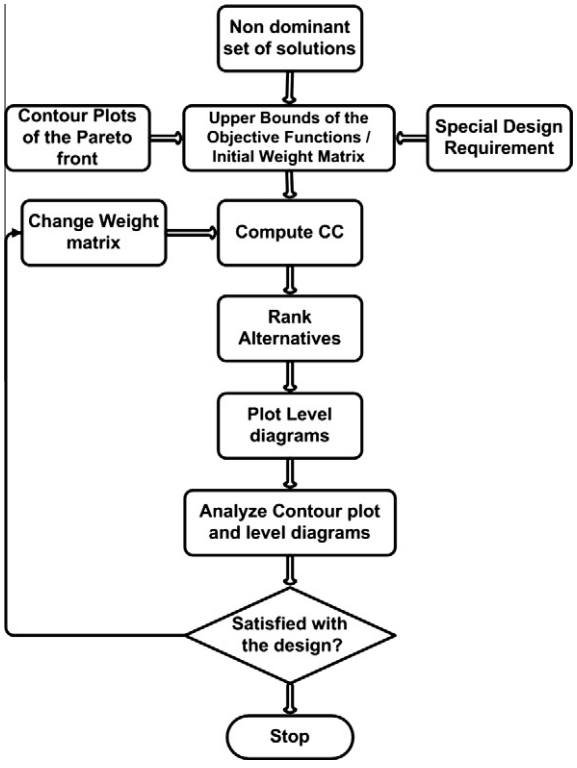

Fig. 10. Block diagram of the MCDM process.

maximum lies in A. Comparison of Case 4 to Case 5 shows that, the global maximum moves from B to A as the weight for the unmet load fraction increases.

Similar to the maxima of the unmet load fraction, the maxima of the LEC, fuel consumption and CC contour plots can be found in Fig. 15, areas C and D. By analyzing Table 16 it can be deduced that the global maximum belongs to Section D. It can be concluded

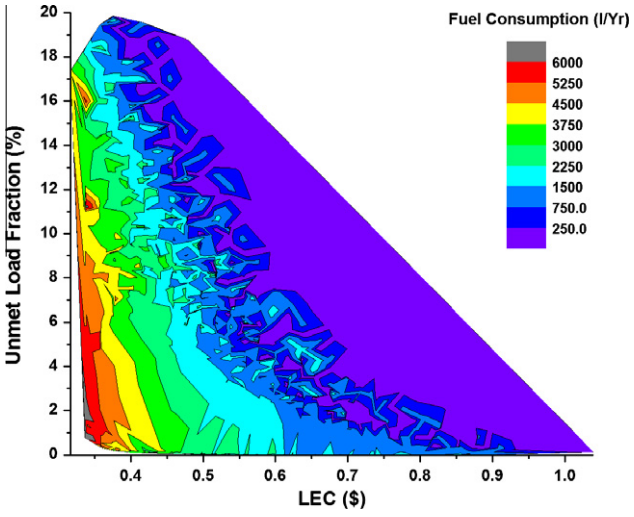

Fig. 11. Contour plot of LEC, unmet load fraction and fuel consumption.

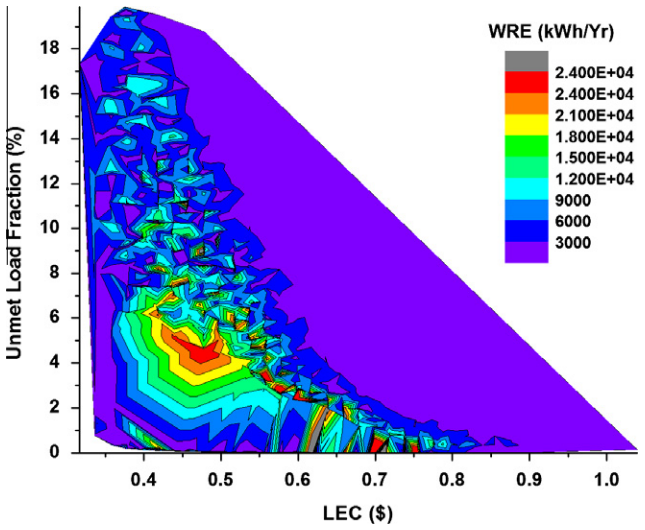

Fig. 12. Contour plot of LEC, unmet load fraction and WRE.

Table 14
Weight matrix for case study.

Rank	LEC	Unmet fraction	Fuel consumption	WRE
Case 4	0.8	0.05	0.1	0.05
Case 5	0.5	0.2	0.2	0.1
Case 6	0.6	0.2	0.1	0.1

that a significant reduction in fuel consumption can be achieved for a marginal increase in LEC with the shift of the global maximum from D to C. However, it is essential to evaluate the impact of reducing the fuel consumption on the other objectives. To that end, a contour plot of unmet load fraction, fuel consumption and CC is constructed (Fig. 16). Two local maxima (F and G) are identified with a global maximum (E). If the weight of fuel consumption is increased, the global maximum of the cost-fuel consumption contour plot moves from D to C, while the global maximum moves from E to G in the unmet load fraction-fuel consumption contour plot, indicating a significant reduction in power supply reliability. Therefore, it is apparent that, although shifting the global maximum from A to D reduces the fuel consumption, according to

Table 13
Upper bounds of objective functions.

LEC ($)	Unmet load fraction (%)	Fuel consumption (l/yr)	WRE (kW h/yr)	N-LEC	N-unmet fraction	N-Fuel consumption	N-WRE
0.55	2	3000	15,000	0.3230	0.1007	0.4557	0.3028

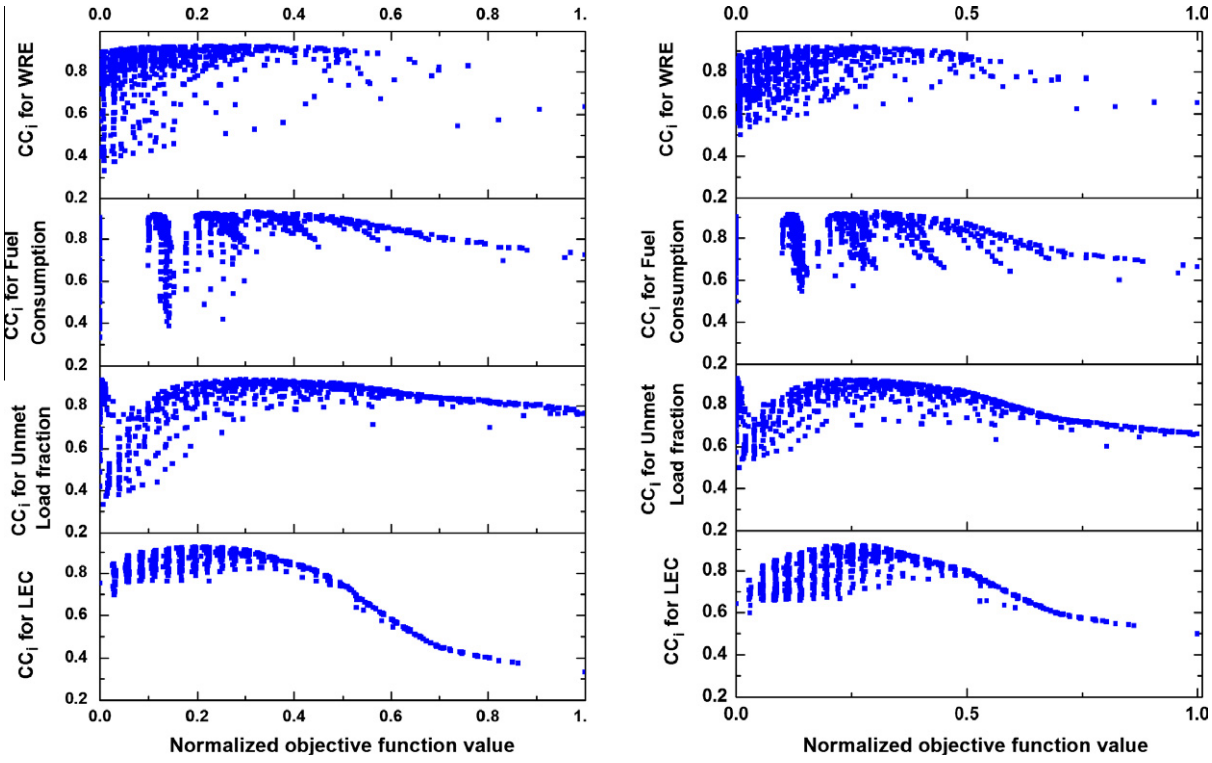

Fig. 13. Level diagrams for Case 4 and Case 5.

Table 15
Top six alternatives for the weight matrix of Case 4.

Rank	N-LEC	N-unmet fraction	N-Fuel consumption	N-WRE	LEC ($)	Unmet fraction (%)	Fuel (L/yr)	WRE (MW h/yr)
1	0.169	0.356	0.320	0.307	0.439	7.07	2105	15,202
2	0.196	0.301	0.324	0.249	0.458	5.98	2134	12,424
3	0.164	0.372	0.335	0.218	0.435	7.39	2202	10,950
4	0.168	0.370	0.324	0.299	0.438	7.35	2134	14,791
5	0.196	0.289	0.306	0.346	0.458	5.74	2015	17,042
6	0.196	0.322	0.330	0.228	0.458	6.40	2172	11,442

Table 16
Top six alternatives for the weight matrix of Case 5.

Rank	N-LEC	N-unmet fraction	N-Fuel consumption	N-WRE	LEC ($)	Unmet fraction (%)	Fuel (L/yr)	WRE (MW h/yr)
1	0.251	0.003	0.303	0.228	0.498	0.057	1997	11,419
2	0.276	0.002	0.273	0.252	0.516	0.031	1796	12,558
3	0.252	0.002	0.322	0.132	0.498	0.041	2118	6840
4	0.278	0.002	0.305	0.134	0.518	0.044	2007	6956
5	0.298	0.002	0.280	0.154	0.532	0.040	1840	7912
6	0.218	0.002	0.332	0.299	0.474	0.049	2184	14,819

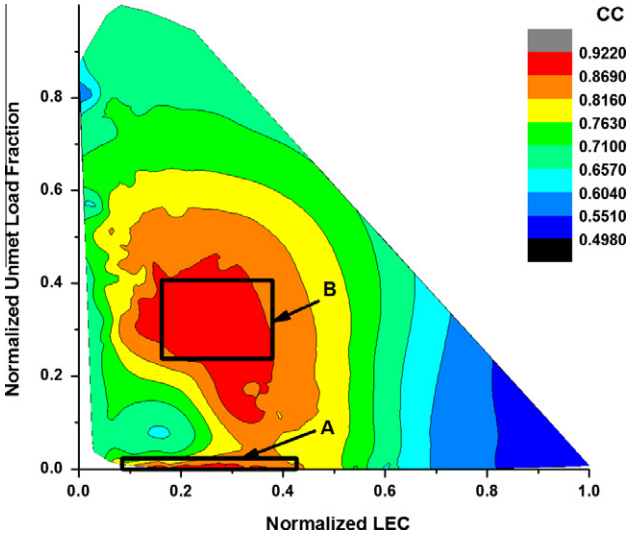

Fig. 14. Contour plot of N-LEC, N-unmet load fraction and CC for Case 5.

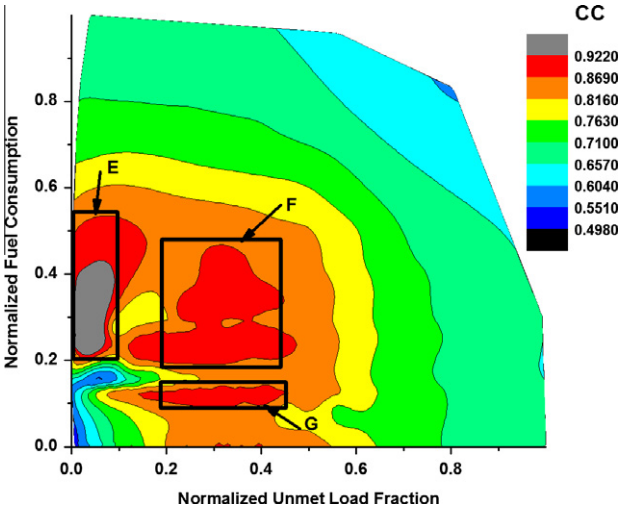

Fig. 16. Contour plot of N-unmet load fraction, N-fuel consumption and CC for Case 5.

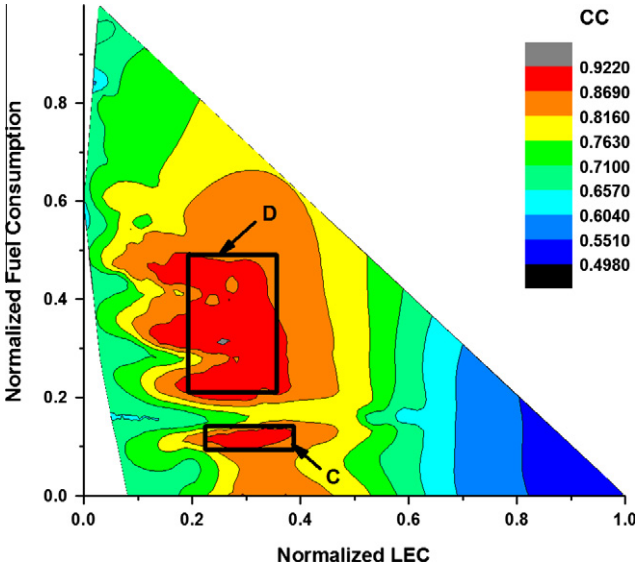

Fig. 15. Contour plot of N-LEC, N-fuel consumption and CC for Case 5.

Fig. 16, it increases the unmet load fraction beyond the upper bounds. However, depending on the application, priority can be given to the objective, and appropriate adjustments can be made. Under these conditions, it is not advisable to reduce fuel consumption while further increasing unmet load fraction and LEC.

With respect to WRE, a gradual variation of CC can be observed, without any local maxima (Fig. 14) where analysis become simpler. The weight matrix and design are finalized (Case 6) after considering several alternative designs. The objective function values and the best six alternatives according to the finalized weight matrix are listed in Table 17.

6. Conclusions

When compared to the classical cost optimization, Pareto multi-objective optimization has the advantage of optimizing several conflicting objectives in the design process to develop a non-dominant set of alternative designs. However, it is essential to move beyond the Pareto set and come up with a final design using MCDM where no previous literature exists. A novel technique is suggested in this paper that combines Fuzzy-TOPSIS with Pareto multi-objective optimization in designing standalone energy systems.

The energy and cash flows of the system throughout the system life cycle are modeled and subsequently simulated to develop the objective functions. LEC, the unmet load fraction, fuel consumption and WRE are chosen as the objective functions, and the Pareto front is computed. Fuzzy TOPSIS is combined with 1-D and 2-D level diagrams to obtain the weight matrix. It is found that 2D level diagrams provide a detailed picture of the decision space, simplifying the decision-making process. The novel technique suggested in this study can even be used with different objective functions for different applications. Furthermore, this technique can be extended to create optimum system designs when designing energy systems with conflicting objectives. However, the uncertainty related to system parameters and input variables are not taken into consideration, either in optimization or in decision making, which is the focus of some current research to be reported at a later date.

Table 17
Top six alternatives for the weight matrix of Case 6.

Rank	D_i^-	D_i^+	CC_i	LEC ($)	Unmet fraction (%)	Fuel (L/yr)	WRE (MW h/yr)	SPV[a] panels	Wind turbines[b]	ICG capacity (kV A)	Battery banks
1	9.37	0.75	0.9257	0.471	0.063	2290	9958	47	5	5	26
2	9.37	0.76	0.9247	0.457	0.070	2327	14,469	35	6	5	23
3	9.32	0.77	0.9241	0.498	0.057	1997	11,419	55	5	5	28
4	9.34	0.77	0.9240	0.498	0.041	2118	6840	65	4	5	27
5	9.34	0.77	0.9240	0.474	0.049	2184	14,819	38	6	5	27
6	9.38	0.79	0.9226	0.459	0.055	2504	8805	41	5	5	27

[a] SPV panels with Amorphous type.
[b] Wind turbine with 5 kW capacity.

Acknowledgments

Authors would like to acknowledge Mr. D.M.I.J. Wickremasinghe Mr. D.V.S. Mahindarathna of University of Moratuwa for their help on developing the computer program, Prof. Ajith de Alwis, University of Moratuwa and Nadeesh Madusanka University of Cambridge for helping the group in various ways. This project is financially supported by Senate Research Committee Grant-University of Moratuwa (SRC/LT/2011/12).

References

[1] Weijermars R, Taylor P, Bahn O, Das SR, Wei Y-M. Review of models and actors in energy mix optimization – can leader visions and decisions align with optimum model strategies for our future energy systems? Energy Strategy Rev 2012;1:5–18.
[2] Fadaee M, Radzi MAM. Multi-objective optimization of a stand-alone hybrid renewable energy system by using evolutionary algorithms: a review. Renew Sustain Energy Rev 2012;16:3364–9.
[3] Baños R, Manzano-Agugliaro F, Montoya FG, Gil C, Alcayde A, Gómez J. Optimization methods applied to renewable and sustainable energy: a review. Renew Sustain Energy Rev 2011;15:1753–66.
[4] Luna-Rubio R, Trejo-Perea M, Vargas-Vázquez D, Ríos-Moreno GJ. Optimal sizing of renewable hybrids energy systems: a review of methodologies. Sol Energy 2012;86:1077–88.
[5] Sayyaadi H, Babaie M, Farmani MR. Implementing of the multi-objective particle swarm optimizer and fuzzy decision-maker in exergetic, exergoeconomic and environmental optimization of a benchmark cogeneration system. Energy 2011;36:4777–89.
[6] Konak A, Coit DW, Smith AE. Multi-objective optimization using genetic algorithms: a tutorial. Reliab Eng Syst Safe 2006;91:992–1007.
[7] Saheb-Koussa D, Haddadi M, Belhamel M. Economic and technical study of a hybrid system (wind–photovoltaic–diesel) for rural electrification in Algeria. Appl Energy 2009;86:1024–30.
[8] Kanase-Patil AB, Saini RP, Sharma MP. Integrated renewable energy systems for off grid rural electrification of remote area. Renew Energy 2010;35:1342–9.
[9] Bekele G, Tadesse G. Feasibility study of small Hydro/PV/Wind hybrid system for off-grid rural electrification in Ethiopia. Appl Energy 2012;97:5–15.
[10] Kaldellis JK. Optimum hybrid photovoltaic-based solution for remote telecommunication stations. Renew Energy 2010;35:2307–15.
[11] Kamel S, Dahl C. The economics of hybrid power systems for sustainable desert agriculture in Egypt. Energy 2005;30:1271–81.
[12] Dalton GJ, Lockington DA, Baldock TE. Feasibility analysis of stand-alone renewable energy supply options for a large hotel. Renew Energy 2008;33:1475–90.
[13] Dalton GJ, Lockington DA, Baldock TE. Case study feasibility analysis of renewable energy supply options for small to medium-sized tourist accommodations. Renew Energy 2009;34:1134–44.
[14] Setiawan AA, Zhao Y, Nayar CV. Design, economic analysis and environmental considerations of mini-grid hybrid power system with reverse osmosis desalination plant for remote areas. Renew Energy 2009;34:374–83.
[15] Nandi SK, Ghosh HR. A wind–PV–battery hybrid power system at Sitakunda in Bangladesh. Energy Policy 2009;37:3659–64.
[16] Díaz P, Arias CA, Peña R, Sandoval D. FAR from the grid: a rural electrification field study. Renew Energy 2010;35:2829–34.
[17] Gupta A, Saini RP, Sharma MP. Steady-state modelling of hybrid energy system for off grid electrification of cluster of villages. Renew Energy 2010;35:520–35.
[18] Zhou W, Lou C, Li Z, Lu L, Yang H. Current status of research on optimum sizing of stand-alone hybrid solar–wind power generation systems. Appl Energy 2010;87:380–9.
[19] Bernal-Agustín JL, Dufo-López R. Simulation and optimization of stand-alone hybrid renewable energy systems. Renew Sustain Energy Rev 2009;13:2111–8.
[20] Erdinc O, Uzunoglu M. Optimum design of hybrid renewable energy systems: overview of different approaches. Renew Sustain Energy Rev 2012;16:1412–25.
[21] Bernal-Agustín JL, Dufo-López R, Rivas-Ascaso DM. Design of isolated hybrid systems minimizing costs and pollutant emissions. Renew Energy 2006;31:2227–44.
[22] Bernal-Agustín JL, Dufo-López R. Multi-objective design and control of hybrid systems minimizing costs and unmet load. Electr Power Syst Res 2009;79:170–80.
[23] Perera ATD, Attalage RA, Perera KKCK. Multi objective optimization of lifecycle cost, unmet load, and renewable energy capacity for an expansion of existing standalone internal combustion generator (ICG) systems. ASME; 2011. p. 1433–40.
[24] Pelet X, Favrat D, Leyland G. Multiobjective optimisation of integrated energy systems for remote communities considering economics and CO_2 emissions. Int J Therm Sci 2005;44:1180–9.
[25] Dufo-López R, Bernal-Agustín JL, Yusta-Loyo JM, Domínguez-Navarro JA, Ramírez-Rosado IJ, Lujano J, et al. Multi-objective optimization minimizing cost and life cycle emissions of stand-alone PV–wind–diesel systems with batteries storage. Appl Energy 2011;88:4033–41.
[26] Perera ATD, Wickremasinghe DMIJ, Mahindarathna DVS, Attalage RA, Perera KKCK, Bartholameuz EM. Sensitivity of internal combustion generator capacity in standalone hybrid energy systems. Energy 2012;39:403–11.
[27] Bhattacharyya SC. Review of alternative methodologies for analysing off-grid electricity supply. Renew Sustain Energy Rev 2012;16:677–94.
[28] Deshmukh MK, Deshmukh SS. Modeling of hybrid renewable energy systems. Renew Sustain Energy Rev 2008;12:235–49.
[29] Klucher TM. Evaluation of models to predict insolation on tilted surfaces. Sol Energy 1979;23:111–4.
[30] De Miguel A, Bilbao J, Aguiar R, Kambezidis H, Negro E. Diffuse solar irradiation model evaluation in the North Mediterranean Belt area. Sol Energy 2001;70:143–53.
[31] Durisch W, Bitnar B, Mayor J-C, Kiess H, Lam K, Close J. Efficiency model for photovoltaic modules and demonstration of its application to energy yield estimation. Sol Energy Mater Sol Cells 2007;91:79–84.
[32] Notton G, Lazarov V, Stoyanov L. Optimal sizing of a grid-connected PV system for various PV module technologies and inclinations, inverter efficiency characteristics and locations. Renew Energy 2010;35:541–54.
[33] Chedid R, Akiki H, Rahman S. A decision support technique for the design of hybrid solar–wind power systems. IEEE Trans Energy Conver 1998;13:76–83.
[34] Dufo-López R, Bernal-Agustín JL. Influence of mathematical models in design of PV–diesel systems. Energy Convers Manage 2008;49:820–31.
[35] Dennis Barley C, Byron Winn C. Optimal dispatch strategy in remote hybrid power systems. Sol Energy 1996;58:165–79.
[36] Piller S, Perrin M, Jossen A. Methods for state-of-charge determination and their applications. J Power Sources 2001;96:113–20.
[37] Downing SD, Socie DF. Simple rainflow counting algorithms. Int J Fatigue 1982;4:31–40.
[38] Dufo-López R, Bernal-Agustín JL. Design and control strategies of PV–diesel systems using genetic algorithms. Sol Energy 2005;79:33–46.
[39] Gupta A, Saini RP, Sharma MP. Modelling of hybrid energy system—Part II: combined dispatch strategies and solution algorithm. Renew Energy 2011;36:466–73.
[40] Deb K, Mohan M, Mishra S. Evaluating the ε-domination based multi-objective evolutionary algorithm for a quick computation of pareto-optimal solutions. Evol Comput 2005;13:501–25.
[41] Laumanns M, Thiele L, Deb K, Zitzler E. Combining convergence and diversity in evolutionary multiobjective optimization. Evol Comput 2002;10:263–82.
[42] Deb K, Beyer H. Self-adaptive genetic algorithms with simulated binary crossover. Evol Comput 1999;9:431–54.
[43] Deb K. An efficient constraint handling method for genetic algorithms. Comput Methods Appl Mech 2000;186:311–38.
[44] Wang J-J, Jing Y-Y, Zhang C-F, Zhao J-H. Review on multi-criteria decision analysis aid in sustainable energy decision-making. Renew Sustain Energy Rev 2009;13:2263–78.
[45] Pohekar SD, Ramachandran M. Application of multi-criteria decision making to sustainable energy planning—a review. Renew Sustain Energy Rev 2004;8:365–81.
[46] Wang T-C, Chang T-H. Application of TOPSIS in evaluating initial training aircraft under a fuzzy environment. Expert Syst Appl 2007;33:870–80.
[47] Zandi F, Tavana M. A fuzzy group quality function deployment model for e-CRM framework assessment in agile manufacturing. Comput Ind Eng 2011;61:1–19.

[48] Aydogan EK. Performance measurement model for Turkish aviation firms using the rough-AHP and TOPSIS methods under fuzzy environment. Expert Syst Appl 2011;38:3992–8.
[49] Lin M-C, Wang C-C, Chen M-S, Chang CA. Using AHP and TOPSIS approaches in customer-driven product design process. Comput Ind 2008;59:17–31.
[50] Peng Y, Wang G, Kou G, Shi Y. An empirical study of classification algorithm evaluation for financial risk prediction. Appl Soft Comput 2011;11:2906–15.
[51] Cavallaro F. Fuzzy TOPSIS approach for assessing thermal-energy storage in concentrated solar power (CSP) systems. Appl Energy 2010;87:496–503.
[52] Kaya T, Kahraman C. Multicriteria decision making in energy planning using a modified fuzzy TOPSIS methodology. Expert Syst Appl 2011;38:6577–85.
[53] Behzadian M, Khanmohammadi Otaghsara S, Yazdani M, Ignatius J. A state-of the-art survey of TOPSIS applications. Expert Syst Appl 2012;39:13051–69.
[54] Blasco X, Herrero JM, Sanchis J, Martínez M. A new graphical visualization of n-dimensional Pareto front for decision-making in multiobjective optimization. Inform Sci 2008;178:3908–24.
[55] Zio E, Bazzo R. Level diagrams analysis of Pareto front for multiobjective system redundancy allocation. Reliab Eng Syst Safe 2011;96:569–80.
[56] Zio E, Bazzo R. Multiobjective optimization of the inspection intervals of a nuclear safety system: a clustering-based framework for reducing the Pareto Front. Ann Nucl Energy 2010;37:798–812.
[57] Reynoso-Meza G, Sanchis J, Blasco X, Herrero JM. Multiobjective evolutionary algorithms for multivariable PI controller design. Expert Syst Appl 2012;39:7895–907.
[58] Hajiloo A, Nariman-zadeh N, Moeini A. Pareto optimal robust design of fractional-order PID controllers for systems with probabilistic uncertainties. Mechatronics 2012;22:788–801.
[59] Zio E, Bazzo R. A clustering procedure for reducing the number of representative solutions in the Pareto Front of multiobjective optimization problems. Eur J Oper Res 2011;210:624–34.
[60] Grigg C, Wong P, Albrecht P, Allan R, Bhavaraju M, Billinton R, et al. A report prepared by the reliability test system task force of the application of probability methods subcommittee. IEEE Trans Power Syst 1999;14: 1010–20.